doi: 10.1111/j.1460-2695.2006.00998.x

Fatigue behaviour of SiC_p-reinforced aluminium composites in the very high cycle regime using ultrasonic fatigue

J. HUANG[1], J. E. SPOWART[2] and J. W. JONES[1]

[1] *Department of Materials Science and Engineering, University of Michigan, Ann Arbor, Michigan, USA,* [2] *Air Force Research Laboratory, Materials and Manufacturing Directorate, Wright-Patterson AFB, Ohio, USA*

Received in final form 9 January 2006

ABSTRACT The fatigue behaviour of a 2009/SiC/15p-T4 DRA composite has been examined in the very high cycle fatigue (VHCF) regime where $10^7 \leq N_f \leq 10^9$ cycles. Ultrasonic fatigue was used to achieve the very high cycle counts. Careful processing yielded a composite with a very homogeneous particle distribution with minimal clustering. Fatigue crack initiation was observed almost exclusively at AlCuFe inclusions with no crack initiation observed at SiC particle clusters. Fatigue lives at a given stress level exhibited minimal scatter and subsurface crack initiation was observed in all cases. This behaviour is consistent with the presence of a low number density of critical inclusions that are responsible for crack initiation very early in fatigue life.

Keywords critical number density of inclusions; discontinuously reinforced aluminium composite; subsurface crack initiation; ultrasonic fatigue; very high cycle fatigue.

NOMENCLATURE

d = gage diameter of specimen
d_i = diameter of inclusion
DRA = discontinuously reinforced aluminium
FEPA = Federation of European Producers of Abrasives
l = gage length of specimen
L_H = homogeneous length scale
MSAAF = multi-scalar analysis of area fractions
N_f = number of cycles to failure
n_i = volume density of inclusions
$P(X)$ = probability of intersecting inclusion
N_i = crack initiation lifetime
$N_{i,s}$ = number of inclusions in surface layer
SA_{gage} = surface area of gage section of specimen
V_{gage} = volume of gage section of specimen
VHCF = very high cycle fatigue

INTRODUCTION

Discontinuously reinforced aluminium (DRA) composites containing silicon carbide particles generally display higher elastic modulus,[1] specific strength,[2] increased resistance to wear and creep,[3–5] and improved high-cycle fatigue behaviour[6–9] while still maintaining good ductility and fracture toughness as compared to their monolithic counterparts. In addition, DRA properties are more isotropic than continuously reinforced composites and they can be processed using standard techniques, such as extrusion and forging.[10] When combined with their low density, these attributes make DRA materials excellent candidates for high-performance structural components in aerospace and transportation industries.[11] The primary design criterion in many of these applications is often specific stiffness, but many of these components are subjected to cyclic loading, making it critical to

Correspondence: J. W. Jones. E-mail: jonesjwa@engin.umich.edu

understand the fatigue behaviour of these materials in order to maximize their safety and performance while minimizing service costs. The low-cycle and high-cycle fatigue behaviours of these materials have been well researched and are fairly well understood, but the service lives of many applications can enter into the very high-cycle fatigue regime (VHCF, 10^7 cycles $\leq N_f \leq 10^9$ cycles). Although the field of VHCF research is currently very active overall, the VHCF behaviour of DRA composites has received relatively little attention to the authors' knowledge.[12]

Previous research on VHCF behaviour has focused mainly on steels[13–16] where fatigue cracks initiated primarily subsurface at defects such as pores and inclusions in contrast to high-cycle fatigue studies in similar materials where initiation typically occurred at the specimen surface. These findings were recently examined by Mughrabi[17] who hypothesized that these critical defects must be present in sufficiently low number density such that they are not likely to exist at the specimen surface. These internal defects may be considered as pre-existing cracks with a size equal to the diameter of the defect. Fatigue failure will occur at the most critical of the subsurface sites if the propagation lifetime is less than the lifetime required to initiate a surface crack by other damage accumulation processes and then propagate it to failure.

The fatigue behaviour of DRA composites, including the role of microstructure in fatigue crack initiation, has been reviewed by Allison and Jones[18] and more recently by Llorca.[19] Fatigue crack initiation has been observed at heterogeneities in the reinforcement distribution, such as particle clusters where local stresses are much higher than in the surrounding material,[6–8] and at large reinforcement particles,[6,7,9] in which likelihood of particle fracture is greater than in smaller particles. Crack initiation at pores and intermetallic inclusions has also been observed.[6,7,9] This suggests that DRA materials that have a more uniform reinforcement distribution (i.e. containing fewer particle clusters or atypically large particles) should display improved fatigue behaviour as compared to materials with a more spatially heterogeneous reinforcement particle distribution, particularly at longer lifetimes where the crack initiation lifetime, N_i, comprises most of the total fatigue lifetime, N_f. As N_i can comprise well over 90% of the total fatigue life at longer lifetimes, the characterization of reinforcement size and distribution should yield a better understanding of fatigue behaviour in these materials in the VHCF regime and can be useful in constructing a more accurate model of fatigue behaviour and, ultimately, life prediction.[20,21]

Recent work has shown that a systematic and quantitative approach to microstructural characterization can yield useful relationships between static mechanical properties and microstructural features such as the level of microstructural homogeneity and, correspondingly, the presence of particle clusters. For example, the multi-scalar analysis of area fractions (MSAAF) technique, originally developed by Spowart *et al.*,[22] was recently used to quantify the spatial homogeneity of differently processed DRA microstructures by measuring the variability of local reinforcement area fractions on a metallographically prepared section.[23,24] The technique yields a single scalar parameter – the *homogeneous length scale*, L_H – which has units of length and represents the microstructural length scale beyond which the microstructure is homogeneous to within a prescribed range. Strong correlations were found between this microstructural parameter and the measured tensile elongations of the DRA specimens. Many other microstructural descriptors have been presented in the literature, from analyses based on Dirichlet and other tessellations,[25–30] interparticle spacings,[31–33] radial distribution functions[34] and n-point correlation functions.[24,35,36] Each of these techniques has merit, and many have shown similar correlations between microstructural heterogeneity and measured mechanical properties in spatially heterogeneous systems, including DRA.

The current study aims to characterize the microstructure and fatigue behaviour of DRA materials in the very long life regime where the effects of microstructural features on crack initiation are expected to be critical. In this paper, we report the results of ultrasonic fatigue studies in the VHCF regime on a DRA alloy processed to yield a uniform distribution of reinforcement particles with minimal clustering. The role of particle clustering in a second material processed to yield a more heterogeneous distribution of reinforcement particles will be described in a future paper. The overall goal of this research is to identify the relationships between microstructural variability and fatigue life that would allow construction of more accurate life prediction fatigue models.

MATERIALS

The material investigated in this study was a 2009/SiC/15p-T4 aluminum metal matrix composite produced by DWA Aluminum Composites, Inc. using powder metallurgy techniques. The matrix composition is listed in Table 1. Individual aluminium, magnesium and copper powders were blended with 15 vol.% FEPA F-1000 grit silicon carbide particles, vacuum hot pressed and then extruded to yield a fully dense product. Extrusion was carried out in two steps to yield a 16-mm-diameter rod, for a final extrusion ratio of 404:1. The extruded rods were then solution heat-treated at 554 °C and naturally aged (T4) for 96 h prior to machining and testing. The

Table 1 Composition of 2009 matrix alloy[a]

Cu	Mg	Si	Fe	Zn	O	Ga	V	Ti	Others, each	Others, total	Al
4.17	1.36	0.11	0.11	<0.01	0.37	0.01	0.02	0.02	<0.05	<0.15	Remainder

[a]DWA composites, Chatsworth, CA.

Table 2 Mechanical properties of 2009/SiC/15p-T4 versus unreinforced 2009 T-4[a]

	E (GPa)	σ_y (MPa)	σ_u (MPa)	Elongation (%)
2009/SiC/15p-T4	105	424	594	9.8
Unreinforced 2009-T4	71	255	358	10

[a]DWA composites, Chatsworth, CA.

mechanical properties of the composite and unreinforced matrix alloy are presented in Table 2.

EXPERIMENTAL PROCEDURE

Microstructural characterization

Metallographic specimens were prepared from as-extruded rods in both transverse and longitudinal planes using a diamond wafering saw. Sections were mounted in resin and manually polished using diamond and alumina abrasive solutions with a final polish using a 0.05 μm alumina suspension. Polished sections were examined in the unetched condition by optical and scanning electron microscopy. Chemical analysis was performed using an EDAX Phoenix XEDS system. In addition to the MSAAF analysis, a standard commercial digital image analysis package was also used to characterize reinforcement particle volume fraction, aspect ratio and particle orientation relative to the extrusion direction.

Ultrasonic fatigue

Data acquisition in the VHCF regime using conventional fatigue methods is not practical because it is prohibitively time intensive. Therefore, ultrasonic fatigue techniques, which allow testing frequencies as high as three orders of magnitude greater than conventional fatigue, were used for this study. Details of the experimental setup for ultrasonic fatigue are described elsewhere.[37] Briefly, in this method, a piezoelectric transducer operating at approximately 20 kHz produces resonant vibration in a standard-sized fatigue specimen. Under resonant conditions, maximum displacement occurs at the specimen ends, while a condition of maximum strain exists in the centre of the gage section. Applied stresses are calculated by converting strains imposed on the specimen using the material modulus of elasticity, and assuming elastic deformation of the specimen. The system is calibrated at low applied displacements using strain gages applied to the specimen centre, augmented by displacement measurements made at test loads by high resolution, non-contacting optical instrumentation (MTI-2000 Fotonic Sensor). During fatigue cycling, the vibration amplitude at the specimen end is monitored using an induction-based vibration gage. This vibration gage delivers an input into a closed electronic feedback loop to maintain a constant applied strain amplitude during testing. Strain levels throughout the gage length were found to vary less than 5%.

Fatigue samples were machined from extruded rods with the dimensions shown in Fig. 1. Specimen gage sections were subjected to a low-stress finishing procedure incorporating three stages of polishing with SiC paper. Fatigue tests were performed under fully reversed loading conditions at ambient temperature at a frequency of approximately 20 kHz. Applied stresses were calculated based on Young's modulus values measured by a resonant frequency technique.[38] Ultrasonic pulse and pause times were carefully controlled and compressed air cooling was utilized continually to minimize heating in the gage section. Samples were cycled until resonant conditions could no longer be satisfied because of changes in specimen compliance resulting from fatigue crack growth or until 10^9 cycles were reached, at which point runouts were declared. Runout samples were retested at higher stress levels until failure occurred.

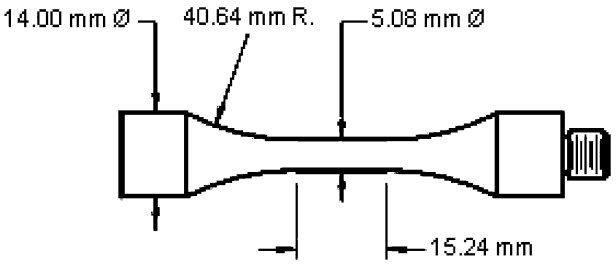

Fig. 1 Ultrasonic fatigue specimen dimensions.

Conventional fatigue

Ten conventional fatigue specimens were also machined from the extruded rods. Sample gage geometry was identical to the ultrasonic fatigue samples with only minor modifications required to facilitate specimen mounting in the MTS Series 810 servohydraulic test frame. Specimen surface preparation specifications were identical to that for the ultrasonic specimens. Stress-controlled axial fatigue tests were performed under fully reversed loading conditions at ambient temperature at a frequency of 30 Hz with a sinusoidal waveform using a servo-hydraulic test system in order to provide a direct comparison with previous conventional fatigue data on similar materials. Samples were cycled to failure or to 10^7 cycles, at which point runouts were declared. Runout samples were retested at higher stress levels until failure occurred.

Analysis of failed samples

The fracture surfaces of failed samples were examined using a Philips XL30FEG SEM to characterize crack initiation features and overall fracture surface morphology. An EDAX Phoenix XEDS system was used for both fractographic analysis and selected compositional mapping of failed samples. Matching fracture surfaces for selected samples were also examined fractographically to document the crack initiation features. Manual serial cross-sectioning was also performed on selected samples to provide additional morphological information about initiation features.

RESULTS

Microstructure

Reinforcement particle distribution and orientation are shown in Fig. 2. Multi-scalar analysis of area fraction (MSAAF) analyses show relatively homogeneous particle distributions with L_H values of 300 μm and 1200 μm for transverse and longitudinal sections, respectively. Additional image analysis results showed a random distribution of particle orientations in the transverse plane and a preferred particle orientation along the direction of extrusion in the longitudinal plane. SiC particle sizes were mildly bi-modally distributed as shown in Fig. 3, with an average equivalent spherical diameter of 2.5 μm. The

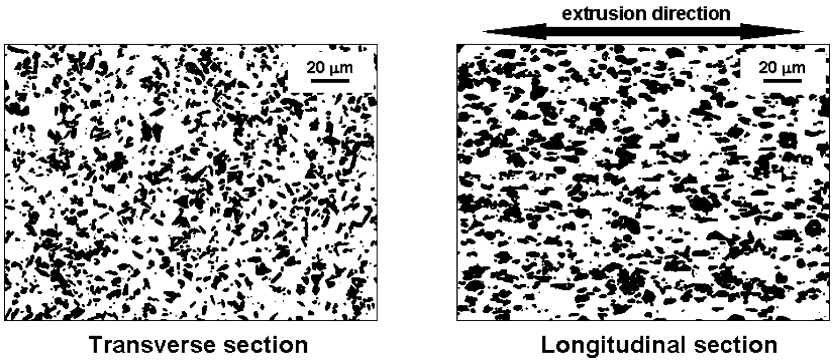

Fig. 2 Transverse and longitudinal microstructure of 2009/SiC/15p-T4.

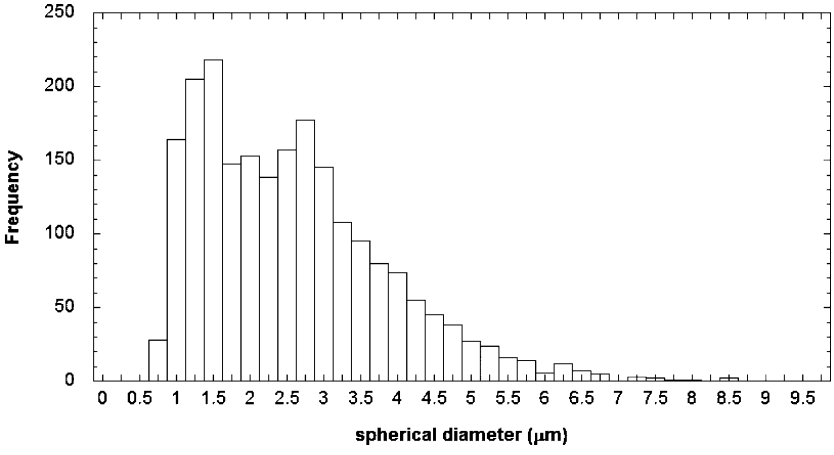

Fig. 3 SiC particle size distribution, showing mildly bimodal statistics. Mean particle diameter is 2.58 μm.

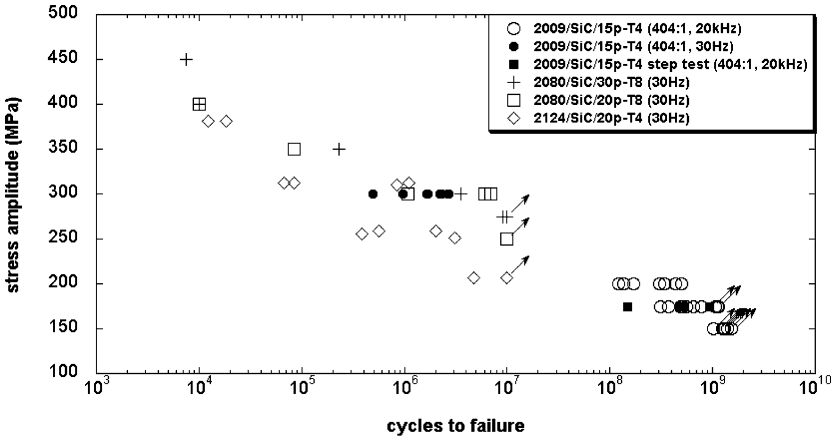

Fig. 4 Ultrasonic fatigue ($N_f > 10^8$ cycles) data compared with conventional fatigue data ($N_f < 10^7$ cycles).

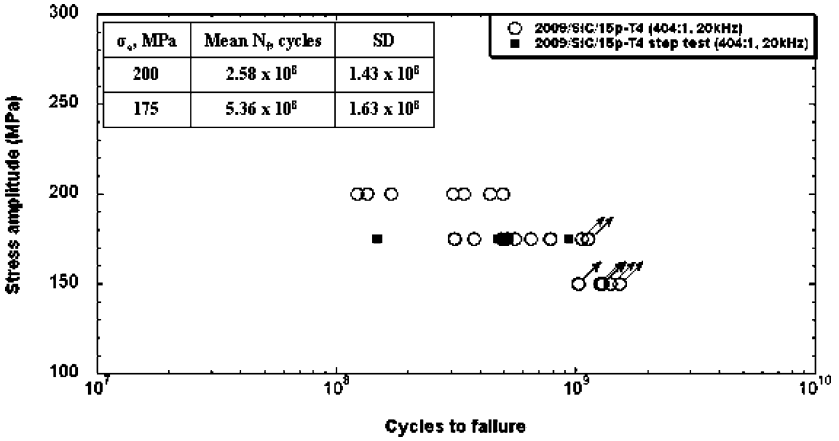

Fig. 5 Ultrasonic fatigue behaviour of 2009/SiC/15p-T4.

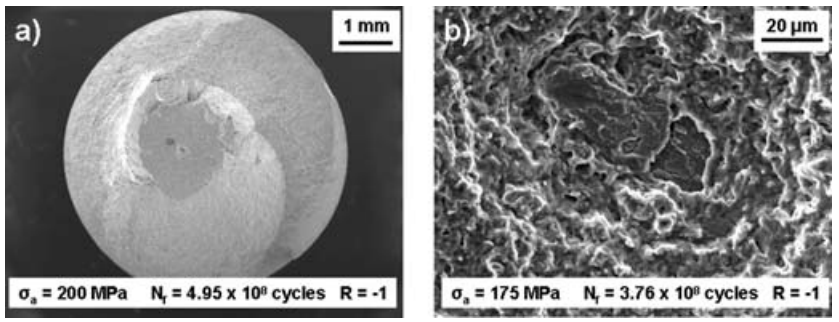

Fig. 6 (a) Subsurface crack initiation, (b) typical initiation feature morphology.

average particle aspect ratio (as defined by the ratio of major to minor axis length for a best-fit ellipse for each particle) was approximately 2:1. Similar results have recently been reported by Ganesh and Chawla[39] for similarly processed 2080/SiC_p DRA materials.

Fatigue behaviour

The VHCF results from ultrasonic fatigue and HCF results from conventional fatigue obtained in the present study are compared in Fig. 4 with conventional fatigue data obtained for similar materials[8,9] using a standard servo-hydraulic system operating at 30–40 Hz. The fatigue lifetimes for conventional test frequencies from the present study agree well with the behaviour observed in the earlier studies. Additionally, the VHCF behaviour from the current study using ultrasonic fatigue is in good agreement with the trend suggested by the data obtained at shorter lifetimes using conventional test techniques.

Conventional fatigue lifetimes were found to have little variability in lifetime, varying less than one order of magnitude at the stress amplitude tested. All ten conventional fatigue samples failed at a stress amplitude of 300 MPa and all failures initiated at the specimen surface at AlCuFe inclusions or other surface defects. No

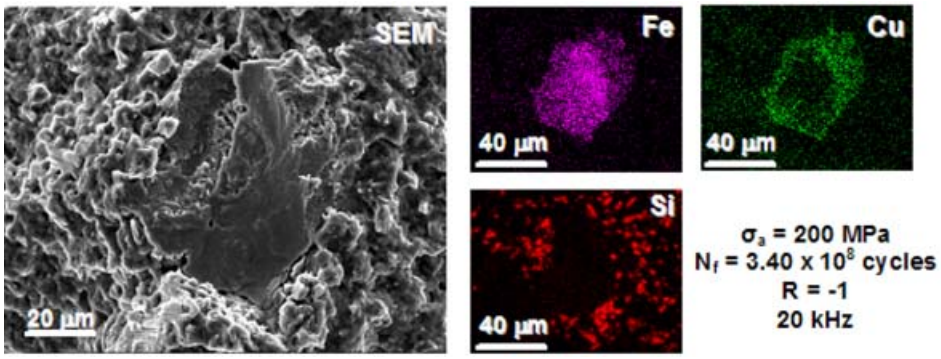

Fig. 7 XEDS compositional mapping identified inclusions as iron aluminide intermetallics.

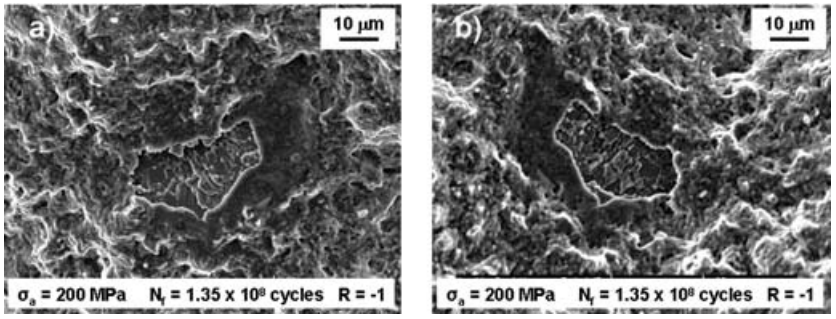

Fig. 8 Matching half fractography of initiation site.

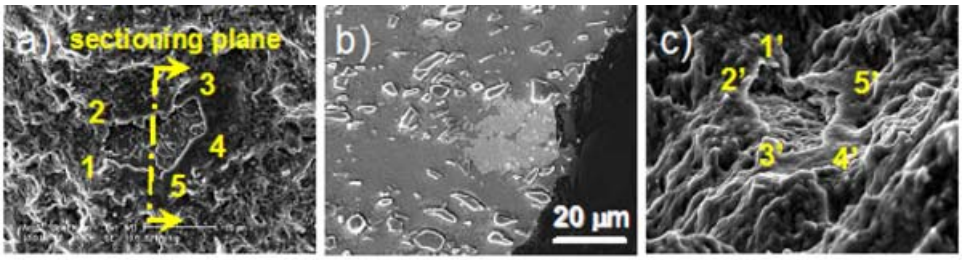

Fig. 9 (a) SEM image of initiating inclusion, (b) cross-section image of inclusion showing incomplete matrix infiltration, and (c) angled matching half image showing depression at initiation site.

initiation at SiC clusters was observed. Further studies of crack initiation behaviour at conventional frequencies are underway.

The fatigue behaviour in the very high cycle regime obtained by ultrasonic fatigue is shown in Fig. 5. Although runouts are typically declared at 10^7 cycles in conventional fatigue tests, fatigue lifetimes approaching 10^9 cycles were measured in the present study. Interestingly, less than one order of magnitude variation in fatigue lifetime, at a given stress amplitude, was observed in the VHCF regime. Twenty-one out of 30 samples failed at the first cyclic stress amplitude tested and all failures initiated subsurface. Fatigue lifetimes at a given stress level followed a standard Weibull distribution. With only one exception, all ultrasonic fatigue failures initiated from a single initiation site and no cracks were observed to initiate from individual SiC particles or clusters of particles. Nearly all ultrasonic fatigue failures initiated at subsurface inclusions and an easily distinguished region of fatigue crack propagation normal to the applied stress, as shown in Fig. 6a, was observed. A typical initiation site is shown in Fig. 6b. Inclusions responsible for crack initiation were observed to be similar in size with a mean diameter of approximately 40 μm. From XEDS compositional mapping, the inclusions were identified as AlCuFe intermetallics and a representative sample is shown in Fig. 7. Fractographic observations suggest that three types of damage to inclusions during processing could result in pre-existing cracks that propagate to failure: (1) inclusions that have fractured and separated, leaving a void in between the two halves, (2) inclusions that have fractured but not separated and (3) inclusions that appear to have decohered from the surrounding matrix. In general, cracking or debonding of these inclusions would be expected to occur when

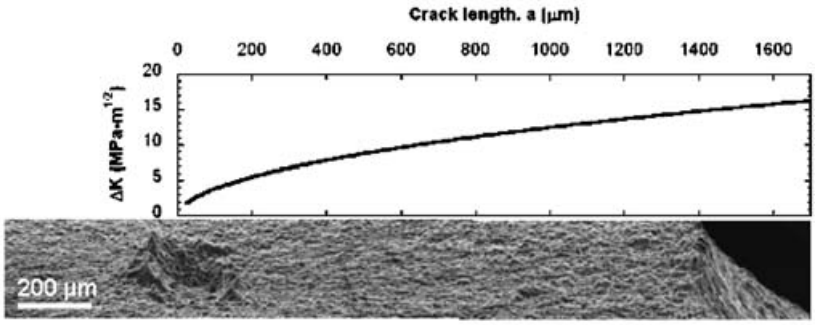

Fig. 10 Fracture surface morphology surrounding initiation site and associated calculated ΔK values.

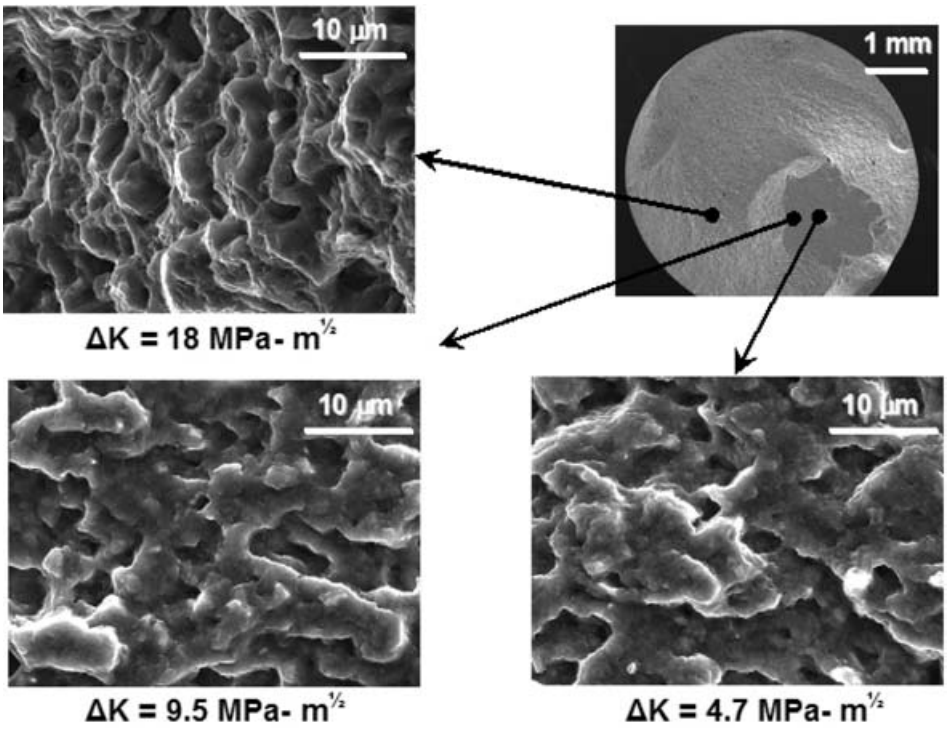

Fig. 11 SiC particles are not visible in the region immediately surrounding the initiation site.

local stresses exceeded the fracture strength or interfacial strength of the inclusion, respectively. At the very low applied stresses of this study (maximum stress amplitude of one third yield stress), however, it is doubtful that the observed damage to these brittle inclusions was due to cyclic loading. Extrusion is known to induce damage in large reinforcement particles resulting from large amounts of plastic deformation.[40–43] Given the very high 404:1 extrusion ratio of the material studied here, it is far more probable that the extrusion process produced these regions of pre-existing damage from which fatigue cracks grew. Extrusion-related damage is particularly apparent in crack initiation sites located at pores in between fractured inclusion halves. In these cases, inclusion separation is accompanied by incomplete matrix infiltration, leaving a void with morphology similar to that of a shrinkage pore. This hypothesis is supported by matching half fractography as presented in Fig. 8, which shows crack initiation about the perimeter of the resultant pore. Additionally, cross-section images show visible matrix intrusion about the fracture surface of the inclusion and SEM images of the sample tilted to 60° also indicate the presence of a depression at the initiation site resembling a shrinkage pore as shown in Fig. 9.

On all failed samples, crack growth in the neighbourhood of the initiation site is extremely tortuous, as shown in Fig. 10. Although the mechanisms responsible for this behaviour are not yet fully understood, it is presumed to be the result of an interaction between the very small crack tip stresses intensities, the small crack sizes and an as-yet undetermined microstructural feature. Decohered or fractured SiC particles are not visible on the fracture surface near the initiation site, but are visible only at the edge of the fatigue crack growth region as shown in Fig. 11. This

is consistent with the findings of Hall *et al.*[9] and suggests that the fatigue crack propagates primarily through the matrix.

DISCUSSION

It should be emphasized that fatigue cracks which propagated to failure in the VHCF regime initiated at inclusions. No evidence was observed for fatigue crack initiation at clusters of SiC particles or at abnormally large SiC particles, as observed in several previous HCF studies on DRA materials.

The incorporation of smaller reinforcement particles into DRA materials process using powder metallurgy, such as in the current material, typically increases the occurrence of SiC particle clusters resulting from the greater tendency of particles to aggregate in the interstices of the matrix powder particles.[44,45] However, simultaneously reducing the matrix powder size has been shown to minimize this effect. Additionally, extrusion has also been shown to homogenize the spatial distribution of reinforcement particles.[42,43] Although the present material utilizes a very small average reinforcement particle diameter (d_p = 2.6 μm), the concurrent reduction in the matrix particle size and the very high final extrusion ratio (404:1) produces a very homogeneous material that displayed minimal clustering of SiC particles in observed metallographic sections. The minimization of this major source of microstructural variability apparently allows the iron aluminide inclusions to become the primary microstructural feature for fatigue crack initiation at the low stress amplitudes used in this study. It may be hypothesized that clusters of reinforcement particles and large intermetallic inclusions are competing mechanisms in fatigue crack initiation in DRA materials and the activation of one over the other may be attributable to their relative sizes and the statistical probabilities of locating one or more of these critical features in the stressed regions.

Iron aluminide inclusions that were smaller than those found to initiate fatigue cracks were readily found by optical microscopy in metallographically prepared transverse sections of ultrasonic fatigue specimens. These inclusions typically appeared in slight contrast relative to the aluminum matrix as shown in Fig. 12. Multiple gage sections were systematically examined for iron aluminide inclusions until at least 100 inclusions were recorded for statistical analysis. Inclusions were modelled as spherical particles for analysis and equivalent section diameters were defined as the smallest circle that could be circumscribed about the inclusion. As shown in Fig. 13, inclusion particle section diameters were found to roughly follow a log-normal distribution as is common for populations of small inclusions. The Schwartz–Saltykov method[46] for determining three-dimensional spherical particle size distributions from two-dimensional data was applied and the results are presented in Fig. 14. The equivalent spherical diameter distribution of inclusions is again found to roughly follow log-normal statistics with a mean inclusion diameter of approximately 9.9 μm (σ = 4.5 μm). Inclusions that were found to initiate fatigue cracks in failed samples were typically 40–50 μm and fall in the long tail of the size distribution, over five standard deviations from the mean. Extreme value statistical analysis methods can be applied in this region to estimate of the number density of these critical inclusions but a reliable level of accuracy would not be attained.

A spatial analysis of initiating inclusions as described by Mughrabi[17] may be adapted to the current study in order

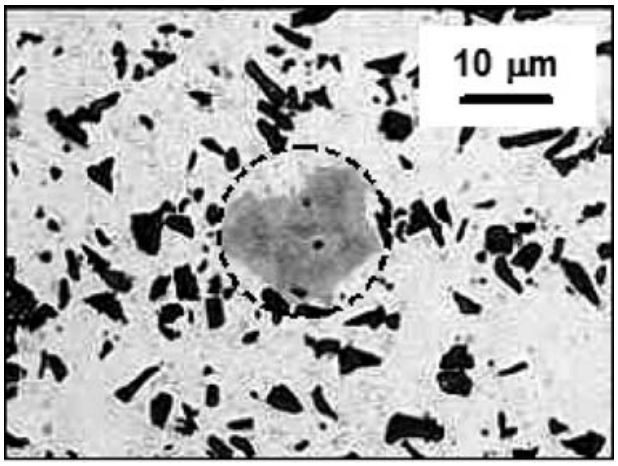

Fig. 12 Optical image of iron intermetallic inclusion as seen in metallographic cross-section.

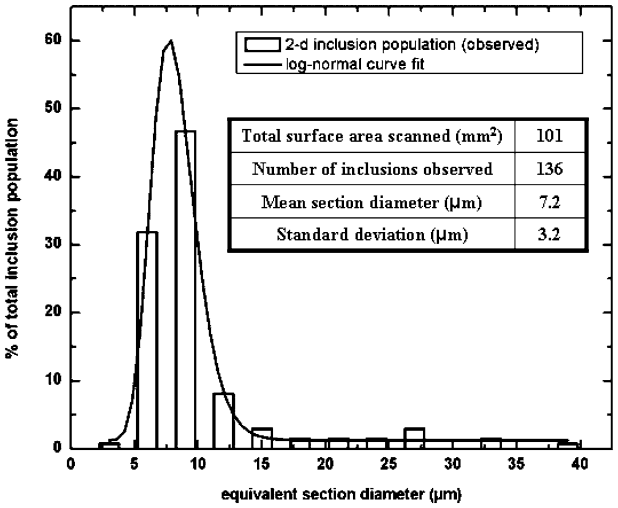

Fig. 13 Equivalent two-dimensional section diameters of inclusions observed in metallographic sections follow a log-normal distribution.

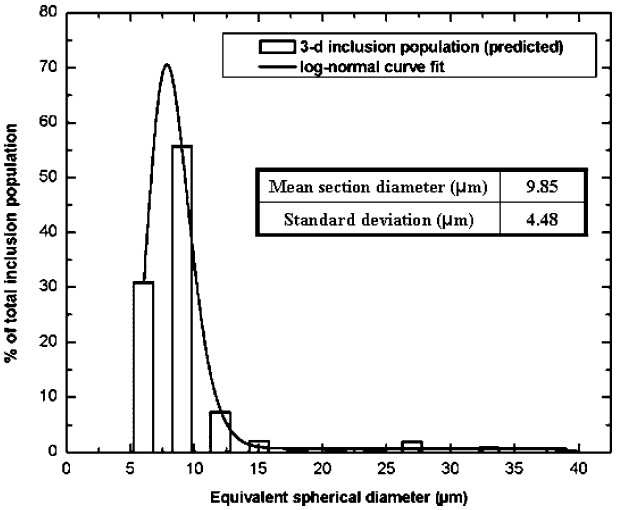

Fig. 14 Equivalent predicted three-dimensional spherical diameters of inclusions as determined using the Schwartz–Saltykov method. Inclusion population follows a log-normal distribution.

to provide a reasonably accurate estimate of the number density of these features. Since the stress intensities at surface inclusions are greater than subsurface inclusions, it is assumed that no critical inclusions lay at the surface of the specimen given the exclusively subsurface crack initiation in this study. Additionally, it is assumed that surface residual stresses are absent. The number of inclusions located at the specimen surface can be defined as:

$$N_{i,s} = n_i \cdot \pi \cdot d \cdot d_i \cdot l,$$

where n_i is the volume density of inclusions of diameter, d_i, in a cylindrical gage section with dimensions d and l. For $N_{i,s} < 1$, n_i must be less than 1.03×10^8 m^{-3}, correlating to fewer than 32 inclusions of critical size in the gage section volume. If the probability of intersecting an initiating inclusion in a random metallographic transverse gage section is defined as[47]

$$P(X \geq 1) = 1 - \left(1 - \frac{(SA_{gage})(d_i)}{V_{gage}}\right)^{n_i V_{gage}},$$

then $P(X \geq 1) = 0.63$. This is consistent with the number densities of critical inclusions suggested by the Schwartz–Saltykov three-dimensional inclusion analysis described above and reinforces the hypothesis that the fatigue life in this material is determined by the presence of low number density inclusions of critical size which, statistically, are located in the subsurface volume.

The presence of these inclusions can also explain the minimal scatter in observed fatigue life at given stresses in the current study. At longer lifetimes, it is well accepted that crack initiation life represents the major fraction of fatigue life. Additionally, the initiation life in high cycle fatigue is typically highly variable given the stochastic nature of microstructural features that can initiate dominant fatigue cracks. However, the unusually low variability in the VHCF lifetimes of the current study suggests that the overall fatigue life is fatigue crack propagation dominated. Pre-damaged inclusions were noted in many fatigue specimens and it may be assumed that these inclusions may serve as pre-existing cracks (i.e. $N_i \sim 0$) with an initial crack size roughly equal to the inclusion diameter. Although pre-existing damage was not observed in all specimens, the overall lack of variability in the fatigue lifetimes and the generally mono-sized nature of the inclusions observed to initiate fatigue cracks suggests that the lifetime required to create a crack equal to the inclusion diameter may also be non-existent or negligible. Therefore, the variability in fatigue lifetime is likely associated with the variation in crack propagation behaviour, which, given the relatively homogeneous microstructure and SiC particle distribution for the highly extruded DRA alloy, should be small. For other structural alloys, where inclusion content and porosity are minimized and a greater fraction of fatigue life is dominated by crack initiation, fatigue lifetime in the VHCF regime can be significantly greater than that observed here.[48]

CONCLUSIONS

The fatigue behaviour in the VHCF regime of a 2009/SiC/15p-T4 aluminum metal-matrix composite with a homogeneous reinforcement particle distribution has been examined using ultrasonic fatigue. Lifetimes in the 10^7–10^9 range agreed well with the trend suggested by previously reported data on similar materials measured at shorter lifetimes and higher stresses using conventional fatigue techniques. Fatigue cracks initiated at intermetallic inclusions and only subsurface initiation was observed in the VCHF regime, suggesting that the number of critical inclusions in the gage volume was sufficiently small to render surface initiation statistically insignificant. The variability in fatigue life in the VHCF regime was small for this material, indicating the likely dominance of crack propagation, rather than crack initiation.

Acknowledgements

The authors would like to acknowledge the following individuals for their valuable assistance in this work: Chris Torbet of the University of Michigan, Dr. Amit Shyam of Oak Ridge National Laboratories, and Cory Smith and Dr. Mark van den Bergh of DWA Aluminum Composites. This project was funded by the U.S. Air Force Office of Scientific Research (Grant No. F49620-03-1-0069), which is gratefully acknowledged.

REFERENCES

1 Nardone, V. C. and Prewo, K. M. (1986) On the strength of discontinuous silicon carbide reinforced aluminum composites. *Scr. Metall.* **20**, 43–48.

2 Wu, Y. and Lavernia, E. J. (1992) Strengthening behavior of particulate reinforced MMCs. *Scr. Metall. Mater.* **27**, 173–178.

3 Wang, A. and Rack, H. J. (1991) Transition wear behavior of SiC-particulate- and SiC-whisker-reinforced 7091 Al metal matrix composites. *Mater. Sci. Engng A, Struct. Mater. Prop. Microstruct. Process.* **A147**, 211–224.

4 Modi, O. P., Prasad, B. K., Yegneswaran, A. H. and Vaidya, M. L. (1992) Dry sliding wear behaviour of squeeze cast aluminum alloy-silicon carbide composites. *Mater. Sci. Engng A, Struct. Mater. Prop. Microstruct. Process.* **A151**, 235–245.

5 Hong, S. H. and Chung, K. H. (1995) High temperature creep behavior of SiC/2124Al metal matrix composites. *Key Engng Mater.* **104–107**, 757–764.

6 Bonnen, J. J., Allison, J. E. and Jones, J. W. (1991) Fatigue behavior of a 2xxx series aluminum alloy reinforced with 15 vol pct SiCp. *Metall. Trans. A* **22A**, 1007–1019.

7 Li, C. and Ellyin, F. (1996) Fatigue damage and its localization in particulate metal matrix composites. *Mater. Sci. Engng A, Struct. Mater. Prop. Microstruct. Process.* **A214**, 115–121.

8 Chawla, N., Andres, C., Davis, L. C., Jones, J. W. and Allison, J. E. (2000) The interactive role of inclusions and SiC reinforcement on the high-cycle fatigue resistance of particle reinforced metal matrix composites. *Metall. Mater. Trans. A, Phys. Metall. Mater. Sci.* **31A**, 951–957.

9 Hall, J. N., Jones, J. W. and Sachdev, A. K. (1994) Particle size, volume fraction and matrix strength effects on fatigue behavior and partice fracture in 2124 aluminum-SiCp composites. *Mater. Sci. Engng A* **183**, 69–80.

10 Hunt, W. H. (2000) Aluminum metal matrix composites today. *Mater. Sci. Forum* **331–337**, 71–84.

11 Hunt, W. H. and Herling, D. R. (2004) Aluminum metal matrix composites. *Adv. Mater. Processes* **162**, 39–44.

12 Sakai, T. and Yasuo, O. (2004) *Proceedings of the Third International Conference on Very High Cycle Fatigue*. The Society of Materials Science, Kusatsu.

13 Wang, Q. Y., Berard, J. Y., Dubarre, A., Baudry, G., Rathery, S. and Bathias, C. (1999) Gigacycle fatigue of ferrous alloys. *Fatigue Fract. Engng Mater. Struct.* **22**, 667–672.

14 Wang, Q. Y., Bathias, C., Kawagoishi, N. and Chen, Q. (2002) Effect of inclusions on subsurface crack initiation and gigacycle fatigue strength. *Int. J. Fatigue* **24**, 1269–1274.

15 Yang, Z. G., Li, S. X., Zhang, J. M., Zhang, J. F., Li, G. Y., Li, Z. B., Hui, W. J. and Weng, Y. Q. (2004) The fatigue behaviors of zero-inclusion and commercial 42CrMo steels in the super-long fatigue life regime. *Acta Mater.* **52**, 5235–5241.

16 Murakami, Y., Yokoyama, N. N. and Nagata, J. (2002) Mechanism of fatigue failure in ultralong life regime. *Fatigue Fract. Engng Mater. Struct.* **25**, 735–746.

17 Mughrabi, H. (2002) On 'multi-scale' fatigue life diagrams and the relevant life-controlling mechanisms in ultrahigh-cycle fatigue. *Fatigue Fract. Engng Mater. Sruct.* **25**, 755–764.

18 Allison, J. E. and Jones, J. W. (1993) Fatigue behavior of discontinuously reinforced metal-matrix composites. In: *Fundamentals of Metal Matrix Composites* (Edited by S. Suresh, A. Mortensen and A. Needleman). Butterworth-Heinemann, Boston, pp. 269–294.

19 Llorca, J. (2002) Fatigue of particle- and whisker-reinforced metal-matrix composites. *Prog. Mater. Sci.* **47**, 283–353.

20 Laz, P. J. and Hillberry, B. M. (1998) Fatigue life prediction from inclusion initiated cracks. *Int. J. Fatigue* **20**, 263–270.

21 Boselli, J., Pitcher, P. D., Gregson, P. J. and Sinclair, I. (2001) Numerical modeling of particle distribution effects on fatigue in Al-SiCp composites. *Mater. Sci. Engng A, Struct. Mater. Prop. Microstruct. Process.* **300**, 113–124.

22 Spowart, J. E., Maruyama, B. and Miracle, D. B. (2001) Mult-scale characterization of spatially heterogeneous systems: Implications for discontinuously reinforced metal-matrix composite microstructures. *Mater. Sci. Engng A, Struct. Mater. Prop. Microstruct. Process.* **301**, 51–66.

23 Spowart, J. E., Ma, Z. Y. and Mishra, R. S. (2003) The effect of friction stir processing (FSP) on the spatial heterogeneity of discontinuously-reinforced aluminum (DRA) microstructures. In: *Friction Stir Welding and Processing II* (Edited by K. V. Jata, M. Mahoney and R. S. Mishra). TMS, Warrendale, pp. 243–252.

24 Tewari, A., Gokhale, A. M., Spowart, J. E. and Miracle, D. B. (2004) Quantitative characterization of spatial clustering in three-dimensional microstructures using two-point correlation functions. *Acta Mater.* **52**, 307–319.

25 Murphy, A. M., Howard, S. J. and Clyne, T. W. (1998) Characterization of severity of particle clustering and its effect on fracture of particulate MMCs. *Mater. Sci. Technol.* **14**, 959–968.

26 Stone, I. C. and Tsakiropoulos, P. (1995) Characterisation of spatial distribution of reinforcement in powder metallurgy route Al/SiCp metal matrix composites. Part 1: Techniques based on microstructure. *Mater. Sci. Technol.* **11**, 213–231.

27 Everett, R. K. and Geltmacher, A. B. (1999) Spatial distribution of MnS inclusions in HY-100 steel. *Scr. Mater.* **40**, 567–571.

28 Lewandowski, J. J. and Liu, C. (1989) Effects of matrix microstructure and particle distribution on fracture of an aluminum metal matrix composite. *Mater. Sci. Engng A, Struct. Mater. Prop. Microstruct. Process.* **107**, 241–255.

29 Bertram, M. and Wendrock, H. (1996) Characterization of planar local arrangement by means of the Delaunay neighbourhood. *J. Microsc.* **181**, 45–53.

30 Yang, N., Boselli, J., Gregson, P. J. and Sinclair, I. (2000) Simulation and quantitative assessment of finite-size particle distributions in metal matrix composites. *Mater. Sci. Technol.* **16**, 797–805.

31 Li, M., Ghosh, S., Richmond, O., Weiland, H. and Rouns, T. N. (1999) Three dimensional characterization and modeling of particle reinforced metal matrix composites. Part 1: Quantitative description of microstructural morphology. *Mater. Sci. Engng A, Struct. Mater. Prop. Microstruct. Process.* **256**, 153–173.

32 Tewari, A., Dighe, M. and Gokhale, A. M. (1998) Quantitative characterization of spatial arrangement of micropores in cast microstructures. *Mater. Charact.* **40**, 119–132.

33 Tao, S. and Boyd, J. D. (1993) Mechanisms of Damage Accumulation and Fracture in Particulate Reinforced Metal-Matrix Composites. In: *Proceedings of the ASM 1993 Materials Congress*. ASM International, Materials Park, OH, pp. 29–40.

34 Louis, P. and Gokhale, A. M. (1996) Computer simulation of spatial arrangement and connectivity of particles in three-dimensional microstructure: application to model

electrical conductivity of polymer matrix composite. *Acta Mater.* **44**, 1519–1528.
35 Torquato, S. (1991) Random heterogeneous media. Microstructure and improved bounds on effective properties. *Appl. Mech. Rev.* **44**, 37–76.
36 Pyrz, R. (1994) Correlation of microstructure variability and local stress field in two-phase materials. *Mater. Sci. Engng A, Struct. Mater. Prop. Microstruct. Process* **177**, 253–259.
37 Mayer, H. R., Lipowsky, H. J., Papakyriacou, M., Roesch, R., Stich, A. and Stanzl-Tschegg, S. (1999) Application of ultrasound for fatigue testing of lightweight alloys. *Fatigue Fract. Engng Mater. Struct.* **22**, 591–599.
38 Yu, C. J. and Prucher, Y. (1993) Measuring Young's modulus and shear modulus – a comparison of dynamic and mechanical techniques. *Adv. Powder Metall. Part. Mater.* **1**, 273–286.
39 Ganesh, V. V. and Chawla, N. (2004) Effect of reinforcement particle orientation anisotropy on the tensile and fatigue behavior of metal-matrix composites. *Metall. Mater. Trans. A, Phys. Metall. Mater. Sci.* **35**, 53–61.
40 Lawrence, C. W., Mummery, P. M. and Tweed, J. H. (1993) Observations of extrusion-induced damage of metal-matrix composites. *J. Mater. Sci. Lett.* **12**, 647–649.
41 Davies, C. H. J. (1995) Critical issues in the extrusion of particle reinforced metal matrix composites. *Key Engng Mat.*, **104–107**, 447–458.
42 Tham, L. M., Gupta, M. and Cheng, L. (2002) Effect of reinforcement volume fraction on the evolution of reinforcement size during the extrusion of Al-SiC composites. *Mat. Sci. Engng A* **326**, 355–363.
43 Cöcen, Ü. and Kazim, Ö. (2002) Ductility and strength of extruded SiCp aluminium-alloy composites. *Compos. Sci. Technol.* **62**, 275–282.
44 Bhanu Prasad, V. V., Bhat, B. V. R., Mahajan, Y. R. and Ramakrishnan, P. (2002) Structure-property correlation in discontinuously reinforced aluminum matrix composites as a function of relative particle size ratio. *Mater. Sci. Engng A, Struct. Mater. Prop. Microstruct. Process* **337**, 179–186.
45 Slipenyuk, A., Kuprin, V., Milman, Y., Spowart, J. E. and Miracle, D. B. (2004) The effect of matrix to reinforcement particle size ratio (PSR) on the microstructure and mechanical properties of a P/M processed AlCuMn/SiCp MMC. *Mater. Sci. Engng A, Struct. Mater. Prop. Microstruct. Process* **381**, 165–170.
46 Underwood, E. (1970) *Quantitative Stereology*. Addison-Wesley Publishing Co., Reading, MA.
47 Yi, J. Z., Gao, Y. X., Lee, P. D., Flower, H. M. and Lindley, T. C. (2003) Scatter in fatigue life due to effects of porosity in cast A356-T6 aluminum-silicon alloys. *Metall. Mat. Trans. A Phys. Metall. Mat. Sci.* **34**, 1879–1890.
48 Szczepanski, C. J., Shyam, A., Jha, S. K., Larsen, J. M., Torbet, C. J., Johnson, S. J. and Jones, J. W. (2005) Characterization of the role of microstructure on the fatigue life of Ti-6Al-2Sn-4Zr-6Mo using ultrasonic fatigue. In: *Materials Damage Prognosis* (Edited by J. M. Larsen, L. Christodoulou, J. R. Calcaterra, M. L. Dent, M. M. Deriso, W. J. Hardman, J. W. Jones and S. M. Russ). TMS, Warrendale, pp. 315–320.

